Nanoparticle-Assisted Stimulated-Emission-Depletion Nanoscopy

Yonatan Sivan,* Yannick Sonnefraud, Stéphane Kéna-Cohen, John B. Pendry, and Stefan A. Maier

The Blackett Laboratory, Department of Physics, Imperial College London, London SW72AZ

ABSTRACT

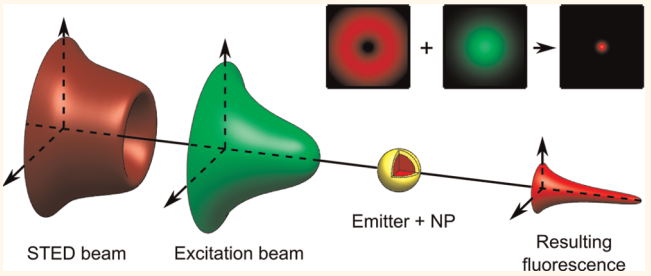

We show that metal nanoparticles can be used to improve the performance of super-resolution fluorescence nanoscopes based on stimulated-emission-depletion (STED). Compared with a standard STED nanoscope, we show theoretically a resolution improvement by more than an order of magnitude, or equivalently, depletion intensity reductions by more than 2 orders of magnitude and an even stronger photostabilization. Our scheme may allow improvement of existing STED nanoscopes and assist in the development of low-power, low-cost nanoscopes. This has the potential to increase the availability of STED nanoscopes and lead to a significant expansion of our understanding of biological and biochemical phenomena occurring on the nanoscale.

KEYWORDS: plasmonics · STED microscopy · super-resolution · nanoshells · photobleaching · triplets

Metal nanoparticles (NPs) have a large variety of applications such as biosensing, nanolasing, solar cells, surface-enhanced Raman spectroscopy and fluorescence enhancement.[1] Specifically, in the context of fluorescence microscopy, metal NPs are used to enhance the excitation and emission rates of weak fluorescent emitters (usually dye molecules), and thus, to improve the overall fluorescence intensity. In fact, low brightness is not the only problem in fluorescence microscopy; it suffers from two additional major problems: limited resolution and poor emitter photostability. Indeed, even scanning confocal fluorescence microscopy, the most important tool for noninvasive deep-tissue imaging,[2] does not allow discerning features that are closer together than allowed by diffraction, approximately half of the emitted light wavelength.[3,4] Thus, biological and chemical processes occurring on a scale smaller than this have been impossible to observe. In addition, fluorescent dyes are unstable due to photobleaching, a process whereby the dye becomes irreversibly inactive, thus, limiting the signal brightness and the scan duration.

In this Article, we propose a novel application for metal NPs in which they are used to improve these two aspects of fluorescence microscopy. Our proposal is based on stimulated-emission-depletion (STED) nanoscopy, a technique that uses stimulated emission to turn off the capability of emitters to emit spontaneously.[5,6] In a typical STED nanoscope, a focused excitation beam is spatially overlapped with a doughnut-shaped beam[7,8] that de-excites emitters to the ground state everywhere except for within the center of the doughnut (Figure 1a), providing *diffraction-unlimited* resolution in the transverse plane.[9] Spectrally, the STED wavelength, λ_{STED}, is red-shifted with respect to the fluorescence emission, see Figure 1b. This minimizes re-excitation by the STED beam and allows a distinction to be made between stimulated emission (at λ_{STED}) and spontaneous emission (around λ_{em}).

STED nanoscopy has already unraveled several key biological phenomena that could not have been discovered otherwise.[10,11] STED also inspired the invention of other techniques providing diffraction-unlimited resolution in fluorescence imaging[12,13] where different mechanisms are used to switch-off the fluorescence. Yet, STED remains by far the fastest technique and the most suitable for tracking the dynamics of small organisms. The STED nanoscope, however, has still not become a widespread tool, mainly because of the high intensities and complicated setup required and the nanoscope's high cost. In addition, STED also suffers from the low brightness and poor photostability of the dyes.

Tremendous progress has been achieved by using a lower excitation-depletion repetition

* Address correspondence to ysivan@imperial.ac.uk.

Received for review March 12, 2012 and accepted April 24, 2012.

Published online April 24, 2012
10.1021/nn301082g

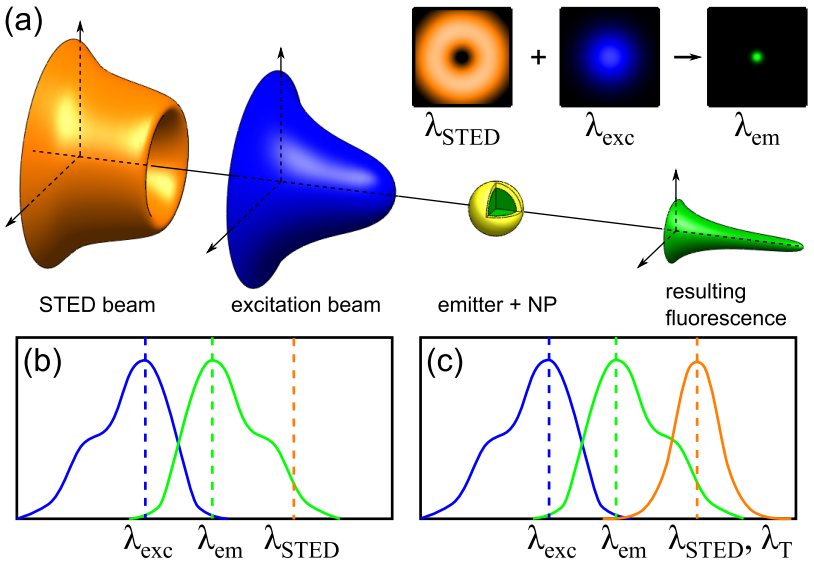

Figure 1. (a) A schematic illustration of a STED nanoscope. Insets show the transverse cross sections of the field distributions and signal. (b) Schematic illustration of the spectral configuration for standard STED measurements specifying the absorption (blue line) and emission (green line) cross sections of the dye, as well as the spectral location of the depletion wavelength λ_{STED} (dashed orange line). (c) Same as panel b for NP-STED measurements with the local-field enhancement associated with the plasmon resonance of the NP (orange line) centered around the depletion wavelength.

rate that minimizes photobleaching and maximizes the depletion intensity,[8] replacing the original pulsed illumination scheme with a continuous wave illumination scheme,[14] and employing time-gating in order to optimize the resolution and reduce the intensity requirements.[15−17]

In this Article, we suggest a *complementary* approach in which instead of modifying the illumination scheme, the fluorescent labels are modified. Specifically, we propose to achieve high depletion intensities by exploiting the near-field enhancement occurring near small metallic nanoparticles. Thus, instead of using standard fluorescent labels (*i.e.*, stand-alone emitters such as dye molecules), we suggest the use of "hybrid" labels that consist of an emitter (or emitters) and a small NP. We refer to our scheme as nanoparticle-assisted STED nanoscopy, or in short, NP-STED.

RESULTS AND DISCUSSION

Principles of NP-STED. Highest field enhancements are attained by tuning the plasmon resonance wavelength of the metal NPs, λ_{PR}, to the depletion wavelength, λ_{STED}, see Figure 1c. Indeed, an emitter placed at nm-proximity to a metallic NP can experience field enhancements of several orders of magnitude at resonance.[1] The depletion will then be correspondingly more efficient for a given incident intensity and the penetration to the tissue deeper. Moreover, the enhancements can allow the use of weaker, hence, cheaper depletion sources. With lower input intensities, there will be less photons incident upon the regions not in the immediate vicinity of the illuminated hybrid label thus reducing photobleaching[8,18,19] and lowering photodamage to the biological environment.[20]

The spectral scheme described above has two additional merits: first, by detuning λ_{STED} from the emission line center λ_{em} it minimizes absorption of the emitted signal. In addition, it can utilize the enhanced absorption in the metal at λ_{PR} to further improve the photostability of the dye. The physical origin of these two effects is the metal-induced enhancement of the emitter's excited state decay rate.[1] This enhancement applies to both the singlet (*i.e.*, fluorescent) and triplet (*i.e.*, phosphorescent) emission; the latter is typically spectrally red-shifted with respect to the fluorescence wavelength λ_{em} by about 100−200 nm. Since λ_{STED} is also red-shifted with respect to the fluorescence (see Figure 1c), with a proper design, it can be matched to the triplet emission wavelength λ_T, thus, leading to a significant enhancement of the nonradiative triplet decay rate, hence, to a shortening of the triplet lifetime and an overall lowering of the triplet state population.

We now recall that in STED nanoscopy, the triplet state population is the main cause for (1) loss of image brightness and contrast due to ground-state depletion[9] and (2) photobleaching.[8,18,21,22] Thus, the emission-depletion detuning allows to transform the detrimental absorption in the metal into an advantage: by maintaining a low triplet state population, it can reduce the effects of photobleaching. Indeed, spectral schemes where the plasmon resonance overlaps the triplet emission λ_T were used before in the context of confocal microscopy and organic semiconductor lasing.[23−25] Then, even rather modest triplet decay rate enhancements have been shown experimentally to lead to significantly weaker photobleaching. Such an improved photostability not only can allow brighter

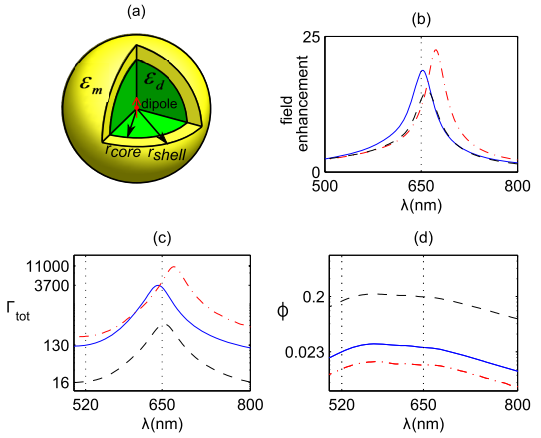

Figure 2. (a) Geometry of the metal nanoshell; (b) electric-field enhancement; (c) total decay rate enhancement; and (d) quantum yield as a function of wavelength for a 52 nm-diameter (black dashed line), 26 nm-diameter (blue line), and 20 nm-diameter (red dash-dotted line) metal nanoshell. Dashed lines denote the enhancement levels at the chosen emission (λ = 520 nm) and depletion ($\lambda \approx$ 650 nm) wavelengths.

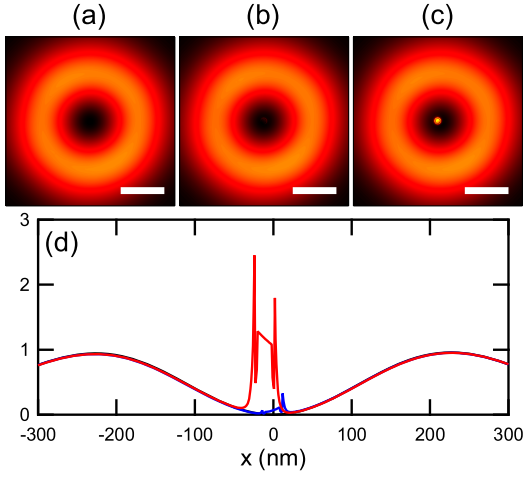

Figure 3. (a) Intensity distribution in the focal plane of an incident Laguerre-Gaussian beam propagating in free space; (b) intensity distribution in the focal plane of a Laguerre-Gaussian beam incident on a small metal nanoshell at the beam center; very little scattering is observed; (c) same as panel b for a metal nanoshell shifted 10 nm away from the beam center. Significant local-field enhancement is observed, yet, the overall doughnut-shaped field pattern is not modified. Scale-bar length is 200 nm. (d) Cross sections along the center for panels a–c with black, blue, and red colors, respectively. In accordance with the local character of the scattering, the different lines are nearly indistinguishable except near the NP.

images and longer scans, but would also allow using higher intensities (hence better resolution)[8] and better contrast[9] compared with standard STED nanoscopy. Importantly, this can be achieved without the need to employ low repetition rates as is customary in standard STED nanoscopy,[8] or more generally, in fluorescence microscopy.[26]

However, the plasmon resonance is sufficiently broad such that there may be some residual enhancement of the nonradiative singlet state decay rate and a corresponding reduction of the fluorescence quantum yield. While the enhanced (spontaneous) decay rate protects the dye from internal conversion and consequent singlet bleaching,[8,27,28] the enhanced decay also competes with the stimulated emission, causing the depletion to be less effective. Specifically, this is manifested through the reduction of the normalized intensity $\zeta = I_{STED}/I_{sat}$ (see Methods), where I_{STED} is the STED intensity and I_{sat} is the saturation intensity, defined as the intensity at which the rates of spontaneous and stimulated emission are equal; since the latter scales with the total decay rate, then, indeed, enhancement of the decay rate corresponds to weaker depletion.

Example: Metal Nanoshells. To quantify these competing effects, we consider, as an example, a configuration of metal nanoshells (*i.e.*, dielectric-core, metal-shell NPs) with a dye emitter placed at the core center[25,27−30] and Figure 2a. Metal nanoshells have several merits. First, there is a wealth of experience in fabricating and using them in biological and medical applications.[31−34] Second, by varying the thicknesses of the core and shell one can tune λ_{PR} across the visible and near-IR spectrum.[30,31] This facilitates matching the plasmon resonance to the STED dye. Third, it offers substantial field enhancements in the core (see Figure 2b) while keeping the emitter at a sufficient distance from the metal so that decay rate enhancement is minimized (Figure 2c) and quenching is not too strong (Figure 2d). Fourth, they have already been shown to result in increased photostability[24,25] which originates from a combination of the enhanced excited state decay rate discussed above and chemcial isolation of the encapsulated dye from oxygen.

The resolution of our scheme is detemined in the following way. First, we calculate the field distribution for a series of relative alignments between the incident doughnut-shaped depletion beam and NP. As seen in Figure 3, the small nanoshell particle does not alter the overall field distribution, and can only induce a local-field enhancement in the immediate vicinity of the NP. The collected signal is then calculated as in ref 9 where each point of the scan constitutes a pixel of the final image. This process mimics the raster scanning used in a STED measurement. For more details and values of parameters used (see Methods).

As a first demonstration, Figure 4a compares the signal obtained from a confocal, STED, and NP-STED imaging schemes at a given depletion intensity. We study a 26 nm-diameter particle with a silica core (r_{core} = 10 nm, ε_d = 2.25) and a gold shell (r_{shell} = 13 nm, dielectric data ε_m taken from refs 35 and 36), chosen due to their biocompatibility and chemical stability.[31] While STED clearly provides a narrower signal, hence, a better resolution than the confocal scheme, the improvement provided by NP-STED is far more significant. For a more systematic comparison, Figure 4b shows the signal width (fwhm) of NP-STED, $d^{(NP)}_{STED}$, as a

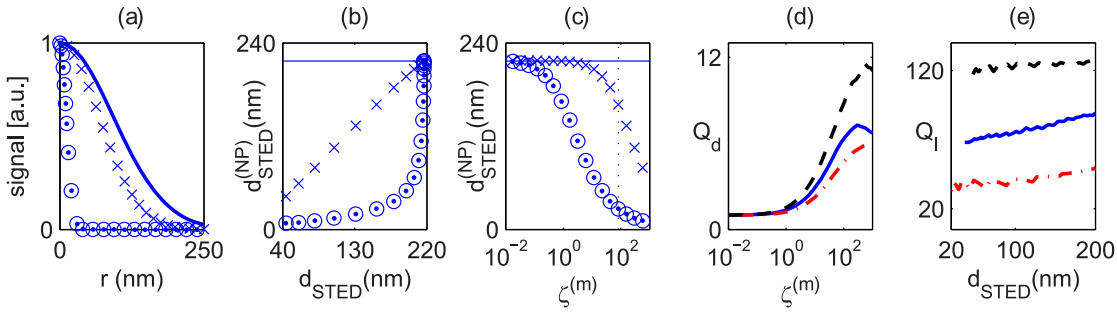

Figure 4. Comparison of resolution obtained using a confocal (solid line), STED (x symbol), and NP-STED (core−shell symbol) imaging schemes. (a) Signal collected from a single emitter at the center of a 26 nm-diameter silica/gold nanoshell; (b) fwhm of the signal as a function of standard STED resolution; (c) same as panel b as a function of peak normalized incident intensity $\zeta^{(m)}$. The vertical dashed line corresponds to the parameters used in panel a. (d) Resolution improvement $Q_d = d_{STED}/d_{STED}^{(NP)}$ and (e) intensity reduction $Q_I = I_{STED}/I_{STED}^{(NP)}$ obtained with nanoshells of a 52 nm-diameter (black dashed line), 26 nm-diameter (blue line), and 20 nm-diameter (red dash−dotted line).

function of the signal width of (standard) STED, d_{STED}. The improved resolution provided by NP-STED is quite striking—up to 7 times better compared with STED (see Figure 4d), thus providing resolution which may even exceed the NP size.

Since in such cases the NP size limits the achieved resolution, one should exploit the (residual) field enhancement for lowering the STED intensities. This is shown in Figure 4c where the resolution provided by both schemes is plotted as a function of the peak normalized depletion intensity $\zeta^{(m)} = \max(\zeta)$. It can be seen that *for any given resolution*, NP-STED requires about 80 times lower intensity compared with STED nanoscopy (see Figure 4e).

As for the signal intensity, we note that for this geometry, the fluorescence quantum yield is reduced by about 28 times at $\lambda_{em} = 520$ nm (see Figure 2d). However, the up to 80-fold intensity reduction should be sufficient to compensate and even overcompensate for that loss by allowing faster repetitions rates, longer scans or stonger excitation levels than in standard STED nanoscopy. Moreover, since the triplet state decay rate is quite high (~3700 times, see Figure 2c), then for a typical phosphorescence yield of $\phi^{(0)} \approx 10^{-4}$ to 10^{-1},[37] we can have $\Gamma_{tot}(\lambda_{STED} \approx \lambda_T)\,\phi^{(0)} \gg 1$, in which case, the triplet population decay rate is enhanced by a factor $\sim \Gamma_{tot}(\lambda_{STED} \approx \lambda_T)\,\phi^{(0)}$.[38] Then, the photobleaching rate is further reduced by about the same factor,[38] thus, providing even further improved photostability.

We also examine the dependence of the improved performance on nanoshell size. As shown in Figure 4d,e, larger nanoshells provide better improvement in imaging performance (*e.g.*, 12-fold improvement of resolution or a 120-fold reduction of required intensities for a 52 nm-diameter nanoshell); this is a result of the lower decay rate enhancement ($\Gamma_{tot}(\lambda_{em}) \approx 16$ compared with ~130 for the 26 nm nanoshell, see Figure 2d). Smaller nanoshells show the opposite trend.

In summary, we have shown that using hybrid fluorescent labels consisting of a dye emitter and a metal NP can lead to a significant improvement in all aspects of the imaging performance of STED nanoscopy. We emphasize that the proposed technique relies on challenging yet demonstrated NP fabrication technology for fluorescence microscopy. Importantly, as the scheme relies on local, *near-field* enhancement rather than on far-field properties such as the scattering cross-section, one can use very small NPs and thus minimize the interference of the NP with the biological processes and exploit the full extent of the resolution improvement. While we restricted the current study to NPs not smaller than 20 nm, there is no physical limitation on using even smaller particles. We further emphasize that our approach is complementary to the improvements made to STED nanoscopes, thus, it is compatible with any STED mode of operation such as CW[14] and time-gated[16,17] STED modes. Moreover, different materials and geometries may also be suitable for NP-STED. The various advantages provided by NP-STED, be these low STED power, high resolution, or improved photostability, allow one to design a NP to suit the imaging requirements and object sizes.

METHODS

In general, the image is acquired by scanning the illumination and depletion beams across the sample and counting the emitted photons for every point of the scan. The total signal arriving at the detector is given by the product of the excitation probability $\eta_{EXC}(I_{EXC}(r,r_0);\lambda_{EXC})$, the spontaneous emission probability $\eta_{SP}(I_{STED}(r,r_0);\lambda_{STED})$, and the detection point-spread-function (PSF) $h_{DET}(r-r_0;\lambda_{21})$; that is,

$$S(r_0) = \int \eta_{EXC}(r, r_0; \cdot)\eta_{SP}(I_{STED}(r, r_0); \cdot)h_{det}(r - r_0; \cdot)\, d^3r \quad (1)$$

Here, r_0 is the center of the illumination beams and r is the coordinate on the sample, both measured with respect to the center of the metal NP. The excitation probability is

given by

$$\eta_{EXC}(r, r_0; \lambda_{EXC}) = F(r)N_1(I_{EXC}(r, r_0); \lambda_{EXC}) \quad (2)$$

where $F(r)$ is the distribution of emitters and N_1 is the number density of the electrons in the excited level. For excitation well below saturation, as is typical, the latter is simply given by the excitation PSF of the microscope. The excitation PSF as well as the detection PSF can be simply estimated as a Gaussian-like functions. The spontaneous emission probability originates from a solution of the rate equations governing the population of the enegry levels of the emitter. In the general case, it was shown that it is given by[9]

$$\eta_{SP}(r, r_0) = \phi_F(r, \lambda_{em})\frac{1 + \gamma(r, r_0)e^{-k_{S,tot}T_{STED}(1+\gamma(r,r_0))}}{1 + \gamma(r, r_0)} \quad (3)$$

where $\varphi_F(r,\lambda_{em})$ is the apparent quantum yield and

$$\gamma(r, r_0) = \frac{\zeta(r, r_0)k_{vib}}{\zeta(r, r_0)k_{S,tot} + k_{vib}} \quad (4)$$

is the depletion factor. The STED intensity

$$\zeta(r, r_0) = \frac{I_{STED}(r, r_0)}{I_{sat}}, \quad I_{sat} = \frac{hck_{S,tot}(r, \lambda_{em})}{\lambda_{STED}\sigma_{em}(\lambda_{STED})} \quad (5)$$

is normalized by the saturation intensity, a level at which the rate of stimulated emission equals the total rate of spontaneous decay, itself defined as

$$k_{S,tot}(r, \lambda_{em}) = k_{S,rad}(r, \lambda_{em}) + k_{S,nrad}(r, \lambda_{em}) \quad (6)$$

where $k_{S,rad}$ and $k_{S,nrad}$ is the radiative and nonradiative decay rates, respectively. Note that all the fluorescence properties are modified by the presence of the metal and become strongly wavelength- and position-dependent. Additional parameters used above are the depletion wavelength λ_{STED}, the emission cross-section of the emitter σ_{em}, the vibrational decay rate k_{vib}, the STED pulse duration T_{STED} and $hc \approx 2 \times 10^{-25}$ Jm.

In the absence of any scattering (*i.e.*, in the absence of NPs), the excitation and depletion fields are translation-invariant, in which case, the signal is given simply by a convolution between the fluorophore distribution $F(r)$ and the product of the emission probability and the excitation and detection PSF. However, in the presence of a scattering element, the field distributions, hence excitation and depletion profiles, depend on the scan coordinate r_0. In this case, the integration in eq 1 cannot be reduced to a simple convolution, so that one has to compute the excitation and depletion fields for each point in the scan. The field distributions are calculated in the frequency domain using rigorous theory for vectorial beam propagation[39] using standard commercial software. The illumination system is assumed to consist of a NA = 1.2 objective lens focusing into water with optimal aperture-filling by the incident beam. The depletion pulse is assumed to be 70 ps long and to have the spatial doughnut profile of a circularly polarized Laguerre–Gaussian beam.[7] Decay rate and quantum yield calculations were performed in the time-domain using standard commercial software.

The emitter was chosen to be a dye molecule having Lorentzian-shaped absorption and emission cross sections with a 50 nm spectral width and a magnitude of 10^{-16} cm^2. The intrinsic emitter lifetime is assumed to be 5 ns, and the intrinsic fluorescence quantum yield is assumed to have the rather high value of $\phi^{(0)} = 0.65$. These values correspond to those of an Atto dye which is popular in STED microscopy. The emission-depletion detuning is chosen to be 130 nm, as in standard STED.

For simplicity, we assume that the system consists of a single metal nanoshell with a single emitter at its center, that is, $F(r) = \delta(r)$. The set of calculations of a scan along the radial direction thus provides a cross-section of the obtained signal. The resolution of the scheme is taken to be the width of signal. We have verified that in absence of metal NPs, this procedure reproduces the well-known confocal PSF and the resolution scaling of STED nanoscopy.[9]

In more realistic cases, the core will be doped with more than one emitter. In this case, one can simply assume a uniform distribution $F(r)$ = Const within the volume containing the emitters (typically smaller than the overall core size). The calculation would be performed in the same way, namely, using eq 1. It can be shown that within the core, the field enhancements are, on average, similar to those experienced by an emitter at the core center; however, the average decay rate enhancement increases. Thus, in the case of a uniform doping of the core, the performance improvement would be somewhat lower than with a single emitter, but the signal will be naturally brighter compared with the case of a single emitter.

Conflict of Interest: The authors declare the following competing financial interest(s): We have submitted a provisional patent application related to the proposal described in the manuscript.

Acknowledgment. Y. Sivan and Y. Sonnefraud would like to thank A. I. Fernández-Domínguez, V. Giannini, P. Török, and P. French for useful discussions. Y. Sivan acknowledges support from the Royal Society and the European Science Foundation. Y. Sonnefraud acknowledges support from the Leverhulme Trust. Y. Sonnefraud and S.A.M. acknowledge support from the EOARD, Grant No. FA8659-09-1-3080.

REFERENCES AND NOTES

1. Giannini, V.; Fernández-Domínguez, A. I.; Heck, S. C.; Maier, S. A. Plasmonic Nanoantennas: Fundamentals and Their Use in Controlling the Radiative Properties of Nanoemitters. *Chem. Rev.* **2011**, *111*, 3888–3912.
2. Lakowicz, J. R. *Principles of Fluorescence Spectroscopy*, 3rd ed.; Springer: New York, 2006.
3. Abbe, E. Beiträge zur Theorie des Mikroskops und der Mikroskopischen Wahrnehmung. *Arch. Mikrosk. Anat.* **1873**, *9*, 413–418.
4. Novotny, L.; Hecht, B. *Principles of Nano-Optics*; Cambridge University Press: Cambridge, UK, 2006.
5. Hell, S. W.; Wichmann, J. Breaking the Diffraction Resolution Limit by Stimulated Emission: Stimulated-Emission-Depletion Fluorescence Microscopy. *Opt. Lett.* **1994**, *19*, 780–782.
6. Klar, T. A.; Jakobs, S.; Dyba, M.; Egner, A.; Hell, S. W. Fluorescence Microscopy with Diffraction Resolution Barrier Broken by Stimulated Emission. *Proc. Nat. Acad. Sci. U.S.A.* **2000**, *97*, 8206–8210.
7. Török, P.; Munro, P. R. T. The Use of Gauss–Laguerre Vector Beams in STED Microscopy. *Opt. Exp.* **2004**, *12*, 3605–3617.
8. Donnert, G.; Keller, J.; Medda, R.; Andrei, M. A.; Rizzoli, S. O.; Luhrman, R.; Jahn, R.; Eggeling, C.; Hell, S. W. Macromolecular Scale Resolution in Biological Fluorescence Microscopy. *Proc. Nat. Acad. Sci. U.S.A.* **2006**, *103*, 11440–11445.
9. Leutenegger, M.; Eggeling, C.; Hell, S. W. Analytical Description of STED Microscopy Performance. *Opt. Exp.* **2010**, *18*, 26417–26429.
10. Willig, K. I.; Rizzoli, S. O.; Westphal, V.; Jahn, R.; Hell, S. W. STED Microscopy Reveals that Synaptotagmin Remains Clustered after Synaptic Vesicle Exocytosis. *Nature* **2006**, *440*, 935–939.
11. Eggeling, C.; Ringemann, C.; Medda, R.; Schwarzmann, G.; Sandhoff, K.; Polyakova, S.; Belov, V. N.; Hein, B.; von Middendorff, C.; Schönle, A.; Hell, S. W. Direct Observation of the Nanoscale Dynamics of Membrane Lipids in a Living Cell. *Nature* **2009**, *457*, 1159–1162.
12. Hell, S. W. Far-Field Optical Nanoscopy. *Science* **2007**, *316*, 1153–1158.
13. Moerner, W. E. New Directions in Single-Molecule Imaging and Analysis. *Proc. Natl. Acad. Sci. U.S.A.* **2007**, *104*, 12596–12602.
14. Willig, K. I.; Harke, B.; Medda, R.; Hell, S. W. STED Microscopy with Continuous Wave Beams. *Nat. Methods* **2007**, *4*, 915–918.
15. Auksorius, E.; Boruah, B. R.; Dunsby, C.; Lanigan, P. M. P.; Kennedy, G.; Neil, M. A. A.; French, P. M. W. Stimulated Emission Depletion Microscopy with a Supercontinuum Source and Fluorescence Lifetime Imaging. *Opt. Lett.* **2008**, *33*, 113–115.

16. Moffitt, J. R.; Osseforth, C.; Michaelis, J. Time-Gating Improves the Spatial Resolution of STED Microscopy. *Opt. Exp.* **2011**, *19*, 4242–4254.
17. Vicidomini, G.; Moneron, G.; Han, K. Y.; Westphal, V.; Ta, H.; Reuss, M.; Engelhardt, J.; Eggeling, C.; Hell, S. W. Sharper Low-Power STED Nanoscopy by Time-Gating. *Nat. Methods* **2011**, *8*, 571–573.
18. Eggeling, C.; Volkmer, A.; Seidel, C. A. M. Molecular Photobleaching Kinetics of Rhodamine 6G by One- and Two-Photon Induced Confocal Fluorescence Microscopy. *Chemphyschem* **2005**, *6*, 791–804.
19. Dyba, M.; Hell, S. W. Photostability of a Fluorescent Marker under Pulsed Excited-State Depletion through Stimulated Emission. *Appl. Opt.* **2003**, *42*, 5123–5129.
20. Hopt, A.; Neher, E. Highly Nonlinear Photodamage in Two-Photon Fluorescence Microscopy. *Biophys. J.* **2001**, *80*, 2029–2036.
21. Eggeling, C.; Widengren, J.; Rigler, R.; Seidel, C. A. M. Photobleaching of Fluorescent Dyes under Conditions Used for Single-Molecule Detection: Evidence of Two-Step Photolysis. *Anal. Chem.* **1998**, *70*, 2651–2659.
22. Bout, D. A. V.; Deschenes, L. A. Single Molecule Photobleaching: Increasing Photon Yield and Survival Time through Suppression of Two-Step Photolysis. *Chem. Phys. Lett.* **2002**, *365*, 387–395.
23. Wang, W.; Xiong, T.; Cui, H. Fluorescence and Electrochemiluminescence of Luminol-Reduced Gold Nanoparticles: Photostability and Platform Effect. *Langmuir* **2008**, *24*, 2826–2833.
24. Hale, G. D.; Jackson, J. B.; Shmakova, O. E.; Lee, T. R.; Halas, N. J. Enhancing the Active Lifetime of Luminescent Semiconducting Polymers *via* Doping with Metal Nanoshells. *Appl. Phys. Lett.* **2001**, *78*, 1502–1504.
25. Zaiba, S.; Lerouge, F.; Gabudean, A.-M.; Focsan, M.; Lermé, J.; Gallavardin, T.; Maury, O.; Andraud, C.; Parola, S.; Baldeck, P. L. Transparent Plasmonic Nanocontainers Protect Organic Fluorophores against Photobleaching. *Nano Lett.* **2011**, *11*, 2043–2046.
26. Donnert, G.; Eggeling, C.; Hell, S. W. Major Signal Increase in Fluorescence Microscopy through Dark-State Relaxation. *Nat. Methods* **2007**, *4*, 81–86.
27. Enderlein, J. Theoretical Study of Single Molecule Fluorescence in a Metallic Nanocavity. *Appl. Phys. Lett.* **2002**, *80*, 315–317.
28. Enderlein, J. Spectral Properties of a Fluorescing Molecule within a Spherical Metallic Nanocavity. *Phys. Chem. Chem. Phys.* **2002**, *4*, 2780–2786.
29. Gordon, J. A.; Ziolkowsky, R. W. The Design and Simulated Performance of a Coated Nano-Particle Laser. *Opt. Exp.* **2007**, *15*, 2622–2653.
30. Miao, X.; Brener, I.; Luk, T. S. Nanocomposite Plasmonic Fluorescence Emitters with Core/Shell Configurations. *J. Opt. Soc. Am. B* **2010**, *27*, 1561–1570.
31. Halas, N. J. The Optical Properties of Nanoshells. *Opt. Photon. News* **2002**, *13*, 26–30.
32. Bardhan, R.; Grady, N. K.; Cole, J. R.; Joshi, A.; Halas, N. J. Fluorescence Enhancement by Au Nanostructures: Nanoshells and Nanorods. *ACS Nano* **2009**, *3*, 744–752.
33. Sun, Y. G.; Xia, Y. N. Gold and Silver Nanoparticles: A Class of Chromophores with Colors Tunable in the Range from 400 to 750 nm. *Analyst* **2003**, *128*, 686–691.
34. Li, W.; Zhang, J.; Zhoub, Y.; Zhang, P. Highly Enhanced Fluorescence of Fluorophores inside a Metallic Nanocavity. *Chem. Commun.* **2011**, *47*, 5834–5836.
35. Palik, E. D. *Handbook of Optical Constants of Solids*; Academic Press: San Diego, CA, 1998.
36. Nehl, C. L.; Grady, N. K.; Goodrich, G. P.; Tam, F.; Halas, N. J.; Hafner, J. H. Scattering Spectra of Single Gold Nanoshells. *Nano Lett.* **2004**, *4*, 2355–2359.
37. Turro, N. J. *Modern Molecular Photochemistry*; Benjamin/Cummings Pub. Co.: Menlo Park, CA, 1978.
38. Kéna-Cohen, S.; Wiener, A.; Sivan, Y.; Stavrinou, P. N.; Bradley, D. D. C.; Horsefield, A.; Maier, S. A. Plasmonic Sinks for the Selective Removal of Long-Lived States. *ACS Nano* **2011**, *5*, 9958–9965.
39. Richards, B.; Wolf, E. Electromagnetic Diffraction in Optical Systems. II. Structure of the Image Field in an Aplanatic System. *Proc. R. Soc. London, Ser. A* **1959**, *253*, 358–379.